Journal of Materials Chemistry B

Accepted Manuscript

ROYAL SOCIETY OF CHEMISTRY

www.rsc.org/materialsB

Journal Name

ARTICLE

Regulating Stemness of Mesenchymal Stem Cells by Tuning Micropattern Features†

Received 00th January 20xx,
Accepted 00th January 20xx

DOI: 10.1039/x0xx00000x

www.rsc.org/

Xinlong Wang,[ab] Tomoko Nakamoto,[a] Ida Dulińska-Molak,[a] Naoki Kawazoe[a] and Guoping Chen*[ab]

Growing evidence suggests that microstructures play an important role in maintenance of multipotency of stem cells. However, it is not clear how micropatterns affect the stemness of stem cells. In this study, we prepared micropatterns of different sizes, shapes and aspect ratios and used them for culture of human bone marrow-derived mesenchymal stem cells (MSCs) to investigate their influences on the stemness of MSCs at single cell level. With the increase of spreading area and aspect ratio, the percentage of cells that were positively stained by stem cell markers decreased. However, cellular geometry controlled by the geometrical micropatterns showed no significant influence on the expression of stem cell markers. Stemness change of stem cells was accompanied with change of nuclear activity and cytoskeleton. The nuclear activity increased with increase of spreading area and aspect ratio. The actin filament structure was significantly influenced by spreading area and aspect ratio. Cells became stiffer when they had sufficient area to spread or were elongated. The results suggested that controlling cell morphology by micropatterns may be useful for variation of stemness of MSCs. This study will inspire the design of materials for maintaining the multipotency of stem cells which would enhance their applicability for clinical use and will help to reveal the process under stem cell quiescence *in vivo*.

Introduction

Stem cells have attracted tremendous attention in tissue engineering and regenerative medicine because of their pluripotency in differentiation to different cell types. Mesencymal stem cells (MSCs) are one of the most commonly used stem cells due to their easy availability, high expansion efficiency and multilineage differentiation.[1-4] Multipotency and self-renewal are the essential characters of stem cells.[5] In vivo, the majority of stem cells are quiescent under homeostasis, but capable to undergo activation upon stimulation.[6] The quiescent state contributes to stem cell maintenance. Stem cells may lose their pluripotency during in vitro expansion culture which limits their application in clinical use.[7] Motivation to maintain the stemness of stem cells during expansion culture has initiated plenty of researches to disclose details of interaction between stem cells and biomaterials.[8-13] Biomaterials can provide various physiochemical and biological cues to interact with stem cells and therefore impact significant influence on stem cells functions. For instance, micropatterns which enabled the geometrical and mechanical control of cell morphogenesis have been extensively used to regulate stem cell survival, proliferation and differentiation.[14] However, the influence of spreading area, aspect ratio and geometry of cells on the stemness of stem cells remains unclear. Thus in this study, we prepared different micropatterns to control the spreading area, geometry and aspect ratio of single stem cells and disclosed the influences of these physical cues on the maintenance of stemness of MSCs.

Materials and methods

Materials

The chemicals and reagents were purchased from Sigma Aldrich unless otherwise noted. Polystyrene tissue culture flasks and dishes were purchased form BD Falcon. MSCGM medium were purchased from Lonza. Human MSCs were obtained from Osiris Therapeutics, Inc. (Columbia, MA) at passage 2. BrdU labeling reagent and the secondary antibodies used for immunofluorescence staining were purchased from Invitrogen™ (Grand Island, NY). 4′,6-diamidino-2-phenylindole (DAPI) mounting medium was purchased from Vector Laboratories, Inc (Burlingame, CA). The primary antibodies mouse anti-CD44s, mouse anti-CD45, mouse anti-CD106 and mouse anti-STRO-1 were purchase from R&D Systems (Abingdon, OX). Rabbit anti-CD11b and rabbit anti-CD73 were purchased from Novus Biologicals (Littleton, CO). Mouse anti-CD19 was purchased from Imgenex (San Diego, CA). Mouse anti-CD105 was purchased from Exbio (Vestec, Czech Republic). Mouse anti-CD34 was purchased from Cayman Chemical (Ann Arbor, Michigan). The secondary antibodies Alexa Fluor 488-conjugated anti-mouse IgG, Alexa Fluor 488-conjugated anti-

[a] Tissue Regeneration Materials Unit, International Center for Materials Nanoarchitectonics, National Institute for Materials Science, 1-1 Namiki, Tsukuba, Ibaraki 305-0044, Japan.
[b] Graduate School of Pure and Applied Sciences, University of Tsukuba, 1-1-1 Tennodai, Tsukuba, Ibaraki 305-8571, Japan.
Email: Guoping.CHEN@nims.go.jp; Fax: +81 029 860 4714; Tel: +81 029 860 4496
†Electronic Supplementary Information (ESI) available: [details of any supplementary information available should be included here]. See DOI: 10.1039/x0xx00000x

mouse IgM and Alexa Fluor 488-conjugated anti-rabbit IgG were purchased from Invitrogen™ (Grand Island, NY). AFM cantilevers were purchased from Bruker (Camarillo, CA) and Novascan Technologies, Inc. (Ames, IA).

Cell purification and culture

The human MSCs were seeded onto a cell culture dish (58.9 cm^2) at passage 2. Around 20 cells were added into each dish and subcultured with MSCGM medium (Lonza Group Ltd.) for 3 weeks to get cell colonies. 0.3% crystal violet was used to stain the formation of colonies. Colonies greater than 4 mm in diameter were collected and subcultured in 25 cm^2 tissue culture flasks for another 3 weeks to get homogeneous cell mass (Fig. 1a-e). The cells were treated with serum free low glucose DMEM medium (starvation) for 24 h to obtain the cells at G0/G1 enriched state. Subsequently the cells were collected and seeded on different micropatterns at a density of 3000 cells/cm^2. The cells were then cultured with low glucose DMEM medium supplemented with 10% FBS and 1% penicillin/streptomycin. The cells attached onto the micropatterned surfaces and spread within the micropatterns to show the same geometries as the underling polystyrene micropatterns.

Preparation and characterization of micropatterns

Photo-reactive azidophenyl-derivatized poly(vinyl alcohol) (AzPhPVA) was synthesized according to previous report.[15,16] The polystyrene plates were cut from tissue culture flask and coated with 0.2 ml of 0.35 mg/ml AzPhPVA solution and then air-dried at room temperature in the dark. The plates were covered with photomasks of different micropatterns and irradiated with UV light (Funa-UV-linker FS-1500) at 0.25 J/cm^2 from a distance of 15 cm. After irradiation, the plates were immersed in Milli-Q water and ultrasonicated to completely remove any unreacted polymer (Fig. 1f). The micropattrens of different sizes, shapes, and aspect ratios were prepared to control the cell morphogenesis which allowed us to investigate the influences of these biophysical features on stemness of MSCs (Fig. 1g). The surface topography of PVA-micropatterned polystyrene plates were characterized by a MFP-3D-BIO atomic force microscope (Asylum Research, Santa Barbara, USA). The micropatterns were sterilized with 70% ethanol followed by aseptic water washing and used for cell culture.

Immunofluorescence staining

Cells were stained for different surface markers to check the multipotency of cells. Cells were fixed with 4% paraformaldehyde for 10 min at room temperature and blocked with 2% BSA and 0.3 M glycine mixture solution for 30 min followed by PBS washing. Primary antibodies were diluted in 1% BSA solution at different concentration according to the protocol. The samples were incubated with the diluted primary antibodies at room temperature for 1.5 h and washed with PBS for three times. Secondary antibody labeling was performed in 1% BSA solution at room temperature for 1 h. Subsequently the cells were permeabilized with 0.2% Triton X-100 in PBS solution for 2 min and stained with Alexa Fluor-594 phalloidin for 20 min. Nuclei were stained with DAPI. The percentage of the cells positively stained with the antibodies was counted with fluorescence microscopy. Only single cell was counted in each experiment and at least 100 single cells were analyzed. Three independent experiments were performed to calculate the means and standard deviations.

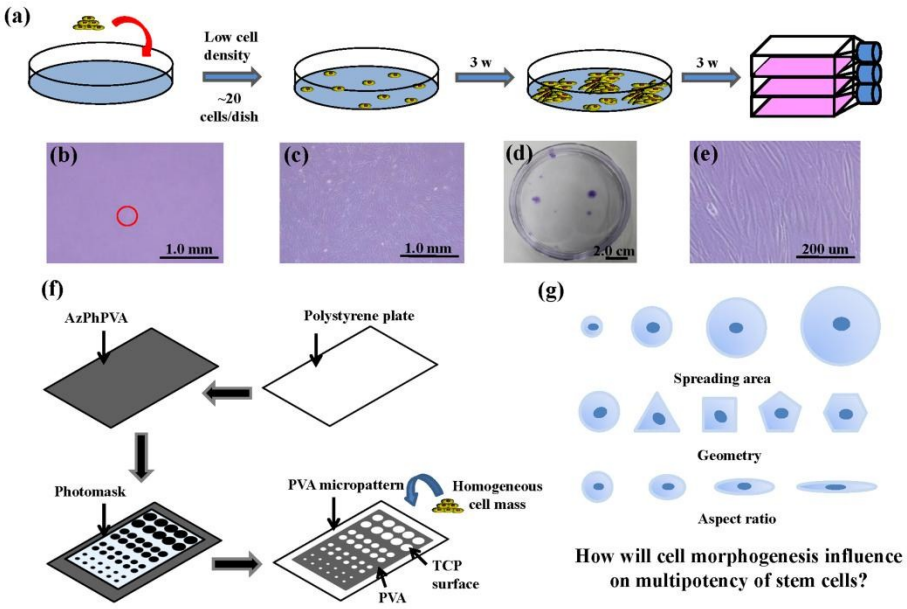

Fig. 1 (a) Purification process of the homogeneous MSCs mass. (b) Phase-contrast micrograph of attached single cell on culture dish. (c) Phase-contrast micrograph of MSCs colony after 3 weeks culture. (d) Photograph of MSCs colonies stained by crystal violet to show their size and distribution. (e) Phase-contrast micrograph of the confluent MSCs form one MSCs colony. The confluent MSCs kept stem cell-like spindle shape. (f) Preparation scheme of the micropatterns. (g) The schematic concept of this research.

BrdU staining

After 6 h culture of MSCs on the micropatterns, non-adherent cells were removed by medium change and low glucose DMEM medium supplemented with 10% FBS, 1% penicillin/streptomycin and 1% BrdU labeling reagent (v/v) was added. After 24 h incubation, the cells were washed with PBS and fixed with 70% ethanol for 30 min followed by PBS washing. Cells were denatured with 2 M HCl for 30 min and then 0.2% Triton X-100 was used to permeabilize cells for 10 min. 2% BSA in PBS solution was used to block the cells for 30 min. Cells were incubated with monoclonal mouse anti-BrdU primary antibody (1:200) at room temperature for 1.5 h and then with Alexa Fluor 488-conjugated anti-mouse IgG antibody (1:500) at room temperature for 1 h followed by PBS washing. Mounting medium with DAPI (Vector) was used to mount the samples and stain the nuclei. The percentage of cells staining incorporation of BrdU was counted by using fluorescence microscopy. Three independent experiments were performed to calculate the means and standard deviations.

Cell mechanics measurement by atomic force microscopy

Cell mechanical properties were measured with a commercially available MFP-3D-Bio AFM microscope. An optical microscope was used to find cells and control the position of the AFM tip. Silicon nitride cantilevers with 600 nm diameter glass ball as a probe were used. Although the cantilevers had nominal spring constant (k = 0.06 N/m), the exact spring constant was measured before each experiment using the thermal tuning method.[17] Force-volume height imaging (FVH) was performed to acquire the cell height map. The scan size was set to 20 pixel × 20 lines at a 80 × 80 μm^2 area. The image was recorded at an indentation velocity of 8 μm/s with a trigger force of 3 nN. The acquiring image was used to select the region of interest where the force curves were collected. All the force curves were obtained at the highest region of cells with a loading rate of 4 μm/s and a trigger force of 3 nN. The samples were immersed in DMEM/HEPES serum medium and measured at room temperature. Live/dead staining was performed after the measurement to detect whether the cells were still alive.

The force curves were fitted to Hertz's contact model to calculate the Young's modulus of cells. According to the probe geometry, parabolic model was used and the formula is given by:

$$F(\delta) = \frac{4}{3} \cdot \sqrt{R} \cdot E_r \cdot \delta^{3/2} \qquad (1)$$

where F is the loading force, R is the radius of the tip, Er is the reduced Young's modulus and δ is the indentation depth. The reduced Young's modulus Er is related with the Young's modulus of sample Es and is given by:

$$\frac{1}{E_r} = \frac{1-\nu_t^2}{E_t} + \frac{1-\nu_s^2}{E_s} \qquad (2)$$

where νt and νs are the Poisson ratios of tips and samples. Since the Young's modulus of tips material (SiO_2) is much greater than that of living cells, equation (2) can be simplified as following:

$$E_r = \frac{E_s}{1-\nu_s^2} \qquad (3)$$

The Poisson ratio of sample is assumed to be 0.5 since cells can be treated as soft incompressible materials.[18]

Results

Preparation and characterization of PVA-micropatterned polystyrene surfaces and purified cell mass

Photo-reactive poly (vinyl alcohol) (PVA) was micropatterned on polystyrene surface using UV photolithography. A transparent quartz slice with interval nontransparent micro-features was used as the photomask (Fig. 2a). Cell adhesive polystyrene (PSt) micropatterns were surrounded by non-adhesive PVA (Fig. 2b). The thin PVA grafted to the substrate surface could resist cells from migrating and spreading across the PSt micropatterns. The height and 3D images of the micropatterns were observed by AFM in Milli-Q water with a contact mode (Fig. 2c, d and Fig. S1). The diameters of the PSt micropatterns and thickness of the grafted PVA layer were analyzed by section analysis (Table S1). The diameters of the PSt micropatterns were nearly the same as those of the designed photomasks indicating good controllability of the micropatterning method. The thickness of grafted PVA varied from 59.66 to 67.98 nm which was effective to constrain cells in the PSt micropatterns. Three types of micropatterns with different spreading areas (Fig. S2), geometries (Fig. S3) and aspect ratios (Fig. S4) were prepared. They were circular micropatterns having a diameter of 20, 40, 60 and 80 μm and a respective surface area of 314, 1256, 2826 and 5024 μm^2; 1134 μm^2 micropatterns having a geometry of circle, triangle, square, pentagon and hexagon; and 706 μm^2 ellipse micropatterns having an aspect ratio of 1, 1.5, 4 and 8. The micropatterns were used for culture of MSCs to systematically compare the influence of different morphogenic cues on stem cells functions.

Human bone marrow-derived MSCs are usually isolated primarily by their tight adherence to plastic culture dishes which will cause the initial heterogeneity.[19] In order to get the homogeneous cell mass, purification of human MSCs was processed based on clonal culture. The initial state of purified MSCs was checked by immunofluorescence staining. The cells expressed CD73, CD105, CD44, CD106 and STRO-1 surface markers which are commonly used to identify MSCs (Fig. S5) while lacked expression of CD11b, CD19, CD34 and CD45 (Fig. S6).[20-22] The purified homogeneous MSCs were used for culture on the micropatterns. The MSCs attached onto the PSt micropatterns and their morphologies were controlled by underlying polystyrene surfaces (Fig. 2e). Single MSCs arrays with different cellular size, geometry and aspect ratio were formed.

Influence of cell morphology on MSCs stemness

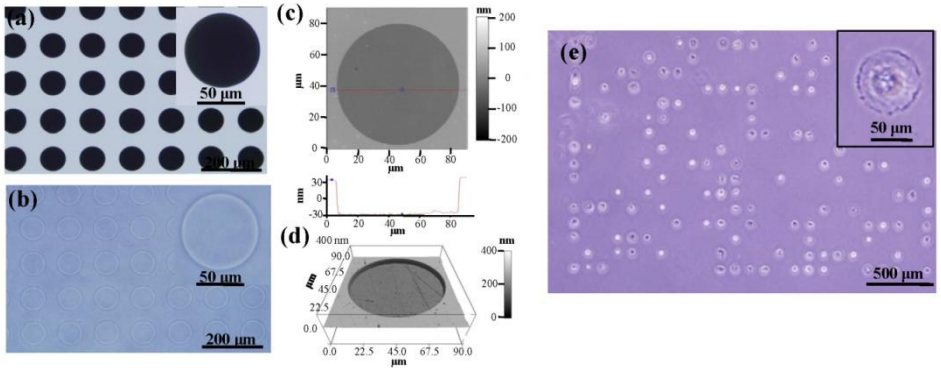

Fig. 2 Characterization of the micropatterns. (a) and (b) are phase contrast micrographs of the photomask and prepared micropattern. The micropattern showed the same geometry as the designed photomask. (c) and (d) are height and 3D images of the circular micropattern with a diameter of 80 µm. The size and depth of the micropattern were well controlled to support for cell attachment and cell morphology confinement as shown by MSCs cultured on circular micropattern with a diameter of 80 µm for 24 h (e).

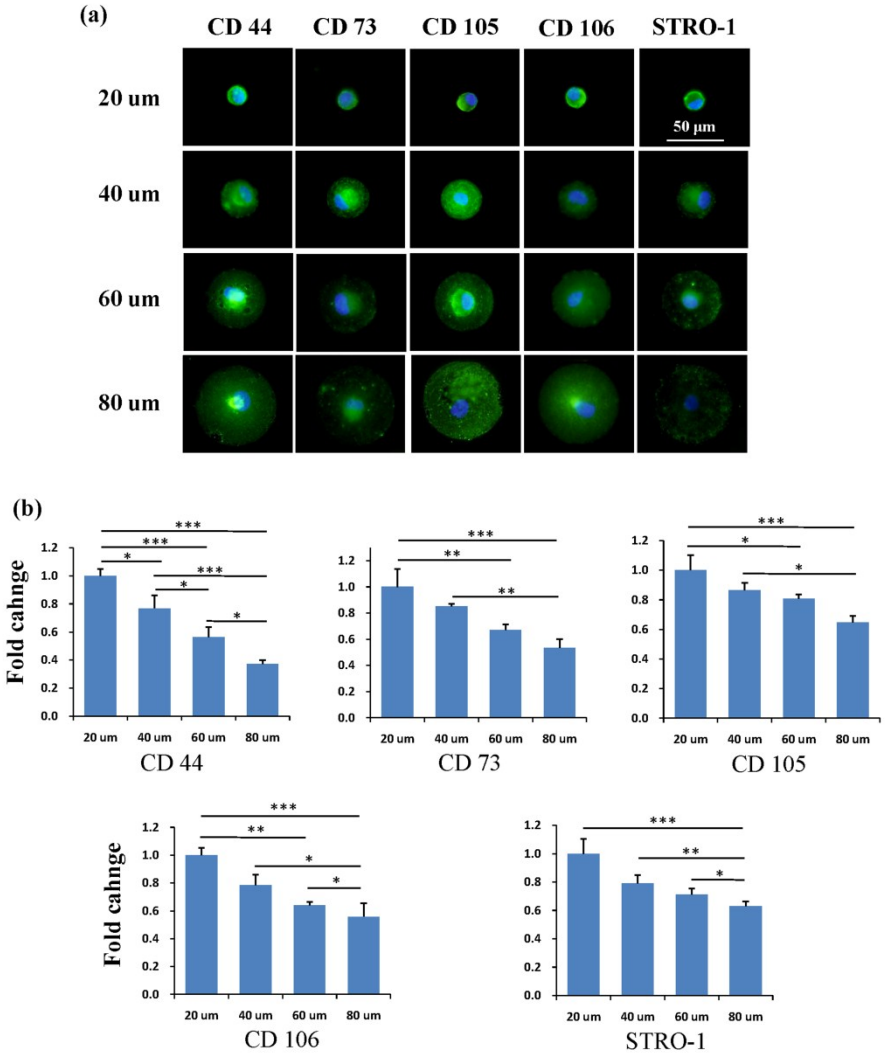

Fig. 3 Influence of spreading area on expression of surface markers of single MSCs. Representative positively stained MSCs with various spreading area (a). Nuclei were stained by DPAI (blue) to distinguish single cell from multiple cells. Surface marker was stained (green) to quantify the percentage of positively stained cells to indicate the stemness of MSCs. Small micropatterned cells exhibited higher expression of CD44, CD73, CD105, CD106 and STRO-1 than large one. In general, the number of positively stained cells decreased with the increase of spreading area indicating loss of multipotency of MSCs (b). The data are represented as the mean ± SD, n > 120. * $p < 0.05$, ** $p < 0.01$ and *** $p < 0.001$.

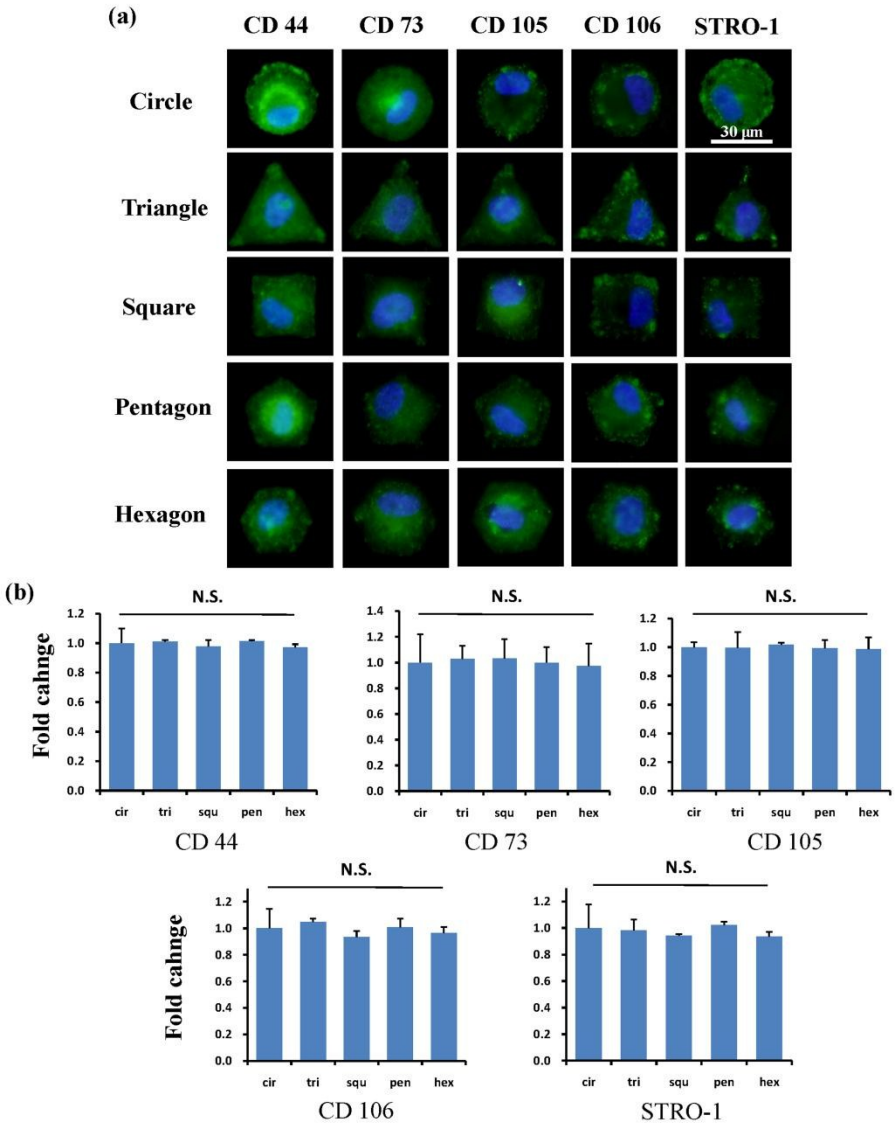

Fig. 4 Influence of cell geometry on expression of surface markers of single MSCs. Representative positively stained MSCs with various geometries (a). Cells assembled strong stress fibers at cell edge while cell central part remained disordered. There was no significant difference of expression of surface makers among cells with different geometries (b). The data are represented as the mean ± SD, n > 120. N.S. means no significant difference.

After MSCs were cultured on the micropatterns for 2 weeks, the stemness of MSCs was analyzed by expression of surface markers of CD44, CD73, CD105, CD106 and STRO-1. Each surface marker was stained and the percentage of positive stained cells was counted to quantify the influence of micropatterns on stemness variation of MSCs. The expression of CD44, CD73, CD105, CD106 and STRO-1 gradually decreased with increase of spreading area (Fig. 3). MSCs cultured on the micropatterns with different geometry expressed similar level of CD44, CD73, CD105, CD106 and STRO-1 (Fig. 4). The expression of CD44, CD73, CD105, CD106 and STRO-1 decreased slightly with increase of aspect ratio. Round cells (AR=1) exhibited significantly higher expression of CD44, CD73, CD105 and CD106 compared to the cells with aspect ratio of 8 or 4 (Fig. 5). The results indicated that the size and aspect ratio of single cell could affect the stemness of MSCs, while shape showed no influence on stemness of MSCs when spreading was limited. Small size and low aspect ratio were good for the maintenance of MSCs stemness.

DNA synthesis of MSCs on micropatterns

Then we turn our attention to reveal the mechanism of the stemness of MSCs tuned by micropatterns. In vivo, stem cells are quiescent with low activity of nucleus and metabolism which endow them superior long-term reconstitution potential.[23] And growing evidences suggest that stem cells in a quiescent state are prone to maintain their multipotency.[24,25] Thus we thought the micropatterns might also affect the stemness through regulation of cell quiescence. To detect the influence of micropatterns on cell quiescence, BrdU staining which reflects the DNA synthesis of the cells was performed (Fig. 6a). The results suggested that spreading area had a significant influence on nuclear activity. With the increase of spreading area, more active nuclei were detected on the

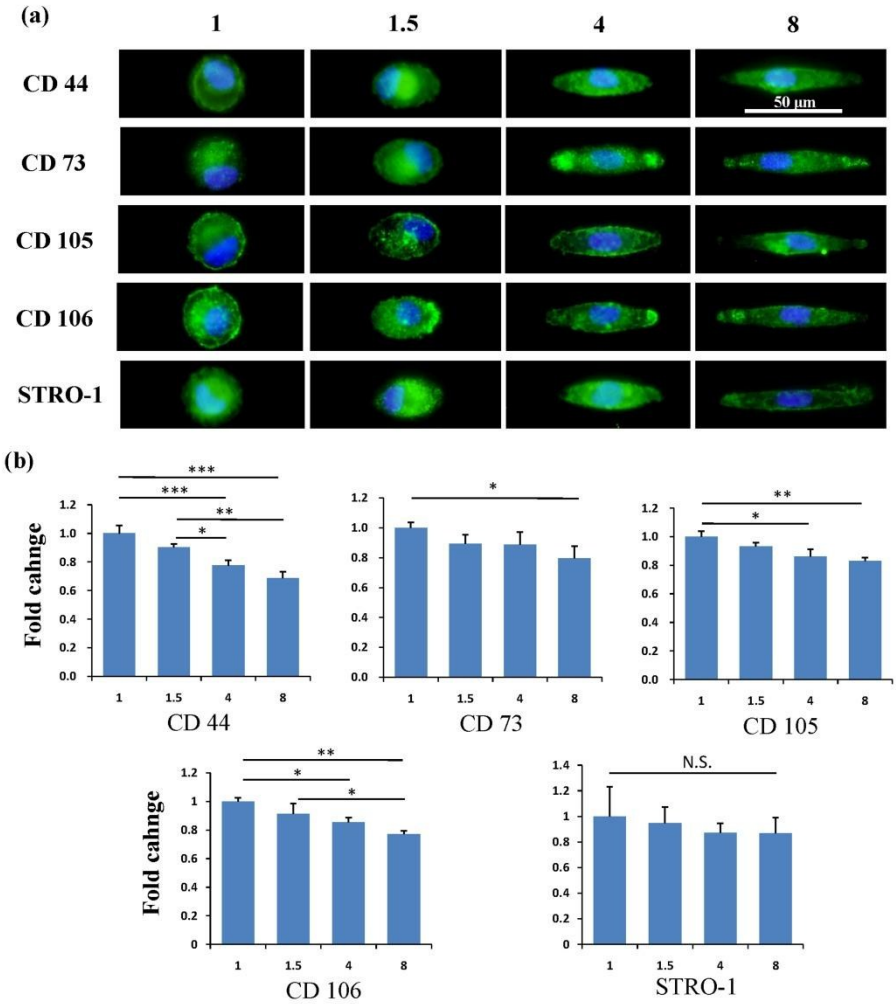

Fig. 5 Influence of aspect ratio on expression of surface markers of single MSCs. Representative positively stained MSCs with various aspect ratios (a). Elongation of cell morphology leaded to pronounced nuclear deformation. Elongated cells had lower expression of surface molecules than circular cells (b). The data are represented as the mean ± SD, n > 120. N.S. means no significant difference, * $p < 0.05$, ** $p < 0.01$, *** $p < 0.001$.

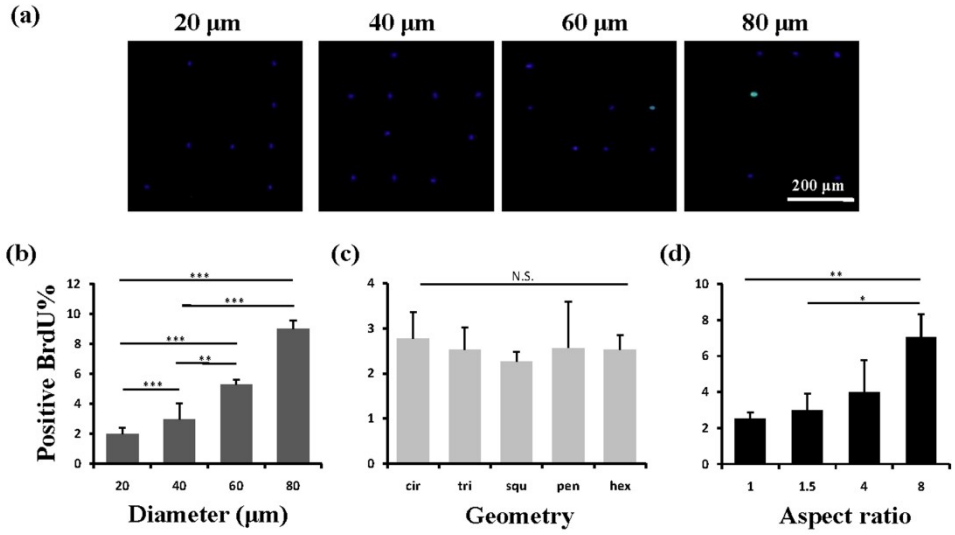

Fig. 6 DNA synthesis activity of MSCs evaluated by BrdU staining. (a) Staining images of cell nuclei cultured on circular micropattrens with a diameter of 20, 40, 60 and 80 μm. Quiescent nuclei were stained by DAPI (blue) and activate nuclei were stained by anti-BrdU (green). With the increase of spreading area, the nuclear activity increased (b). Cells with various geometries had similar nuclear activity (c). More positively stained nuclei were found in elongated cells (d). The data are represented as the mean ± SD, n > 120. N.S. means no significant difference, * $p < 0.05$, ** $p < 0.01$, *** $p < 0.001$.

micropatterns (Fig. 6b). However, the cells cultured on micropatterns with different geometries but same spreading area did not show significant difference of BrdU staining (Fig. 6c). Elongation of cells with the same spreading area resulted in gradual enhancement of nuclear activity. When aspect ratio reached to 8, the cells had significantly higher nuclear activity than the round (AR = 1) or ellipse (AR = 1.5) cells (Fig. 6d). Therefore, we concluded that single MSC with small size or low aspect ratio preferred to keep a quiescent state with low nuclear activity which contributed to the maintenance of MSCs stemness.

Influence of cytoskeleton on cell mechanics

The next question is how the micropatterns modulated nuclear activity. Previous study showed that cells responded to biophysical stimuli through reorganization of cytoskeleton.[26] F-actin filaments can bind to the nuclear envelope anchoring proteins and generate force to the nucleus to influence its state.[27] Therefore, we thought that the micropatterns should regulate the cytoskeleton and influence the cell mechanical state which activated or passivated nuclear activity and finally determined the stemness of MSCs. To confirm this hypothesis, we firstly investigated the cytoskeleton architecture of single MSCs arrays on the micropatterns from their F-actin staining images. The F-actin structure of single MSCs was significantly influenced by spreading area (Fig. 7a). The circular cells with large spreading area assembled their actin filaments in both radial and concentric directions of the circle. With the decrease of spreading area, the radial filaments gradually disappeared and the concentric filaments only assembled at cell periphery. MSCs cultured on the micropatterns with different geometries showed similar actin organization (Fig. 7b). The micropatterned cells predominately assembled their actin filaments at the periphery of the cells and the formed stress fibers stretched along the edges of micropatterns, while no ordered filament structure was found at the central region of cells. Aspect ratio showed significant effect on F-actin structures. Unlike in circular cells, actin filaments in elongated cells were parallel along the long axis of the cell and spanned over the nucleus (Fig. 7c). Not only the cytoskeleton, the nuclear geometry was also elongated dramatically with increase of aspect ratio and oriented towards the direction of long cell axis.

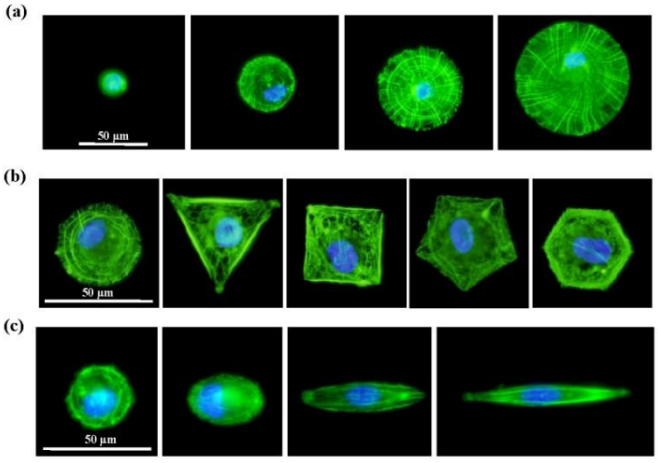

Fig. 7 F-actin staining of MSCs cultured on micropatterns with various spreading areas (a), geometries (b) and aspect ratios (c). MSCs cultured on circular micropatterns with large spreading area exhibited highly ordered actin network. With the decrease of spreading area, the actin filaments were weakened and became randomly orientated (a). Cells with different geometries formed strong stress fibers at cell edge, while disrupt actin assembly observed at cell center (b). With the increase of aspect ratio, MSCs formed straight stress fibers along the long axis of cells (c).

Table 1 Young's modulus of living MSCs cultured on different micropatterns.

Size	E (kPa)	Shape	E (kPa)	AR	E (kPa)
20 μm	0.82 ± 0.65	circle	0.96 ± 0.61	1	0.89 ± 0.60
40 μm	0.99 ± 0.71	triangle	0.97 ± 0.64	1.5	0.93 ± 0.65
60 μm	1.22 ± 0.65	square	0.95 ± 0.63	4	1.16 ± 0.68
80 μm	1.38 ± 0.94	pentagon	0.97 ± 0.59	8	1.23 ± 0.69
		hexagon	0.96 ± 0.64		

Cell mechanics which depends on cytoskeleton structure was then measured by AFM nanoindentation. The AFM measurement of each cell was finished within 1 h to guarantee the cell viability and all the cells attached on the micropatterns were alive after the measurement. The obtained force curves were used to calculate the Young's modulus of cells according to Hertz's model. The final Young's modulus value was determined by fitting the Gaussian function to the histogram created from all the collected data (Fig. 8). The center of the fitting curve represented the average value of the Young's modulus and the half width at the half height was the standard deviation. The histogram became wider with the increase of spreading area but showed similar shape for the cells with various geometries and aspect ratios. Table 1 shows the obtained Young's modulus of MSCs. The results indicated that Young's modulus of MSCs was regulated by their F-actin structure which assembled according to the micropattens. MSCs with large spreading area formed more stress fibers which assembled in radial and concentric directions of the circle. The highly ordered actin structure resulted in a higher elasticity of the cells. With the decrease of spreading area, cells became soft. While for cells having different geometries but same spreading area, they showed similar Young's modulus. The parallel stress fibers formed in elongated cells also increased the Young's modulus of MSCs.

Discussion

Maintenance of multipotency of stem cells is becoming an attractive topic and various methods have been used to investigate the self-renewal of stem cells. A recent study reported that long time culture of MSCs on a hard unpatterned

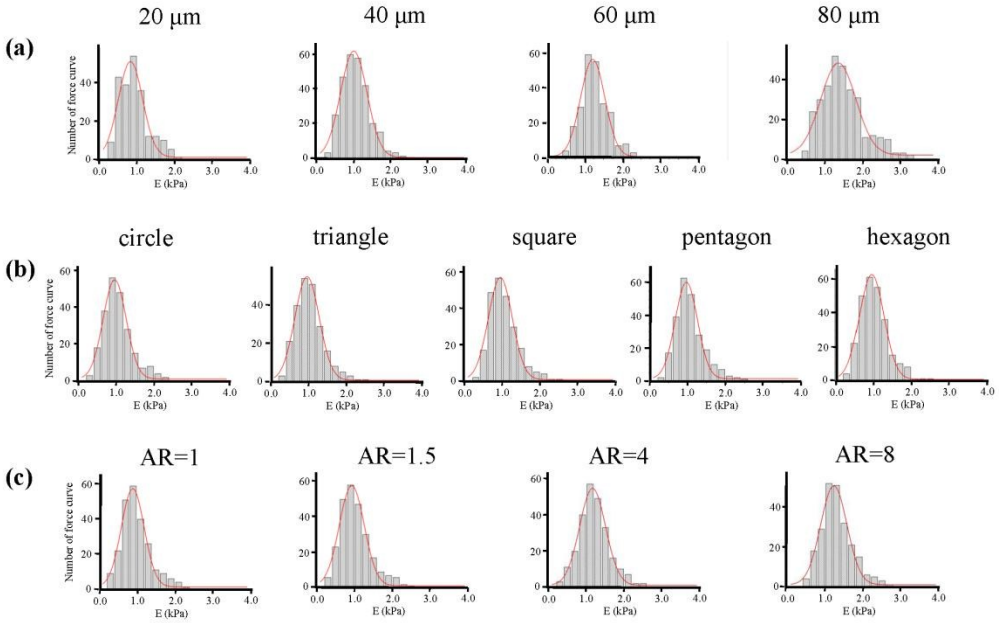

Fig. 8 Histogram of the value of Young's modulus with Gaussian fittings obtained for MSCs cultured on micropatterns with various spreading areas (a), geometries (b) and aspect ratios (c). The data were obtained at 200 nm indentation depths. Bin size: 0.2 kPa (n > 200).

surface would cause a irreversible effects on stem cell fate by activating YAP and RUNX2 in nucleus.[28] The mechanical dosing effects reminding us that it would be difficult to preserve multipotency of stem cells only use conventional tissue culture plates. In this study, micropatterns with different sizes, geometries and aspect ratios were used for culture of MSCs at single cell level to investigate how these physical cues affect the stemness of stem cells and cytoskeleton change. After two weeks culture on the micropatterns, the expression of CD44, CD73, CD105, CD106 and STRO-1 decreased with increase of spreading area and aspect ratio of MSCs, while kept at similar level in cells with different geometry.

The nuclear activity of the micropatterned cells increased with the increase of spreading area. It is well agreed that spreading area as a crucial parameter of the nuclear deformation process can enhance cell proliferation. Increasing in spreading area leads to the enlargement of nucleus which activates DNA synthesis.[29] Meanwhile, cells need to maintain an intact actin cytoskeleton which increases cell contraction at the critical time point in the late G1 phase of cell cycle to enter S phase.[30] The ordered actin structure observed in large cells could fulfil this requirement. When being cultured on the micropatterns of different aspect ratios, the elongated cells assembled their parallel actin filaments throughout the cells. And the perinuclear actin filaments formed a cap which has been reported to stimulate cell proliferation.[31-33] On the other hand, the non-elongated cells only assembled their actin filaments at cell periphery. There were few actin filaments at the perinuclear space. Therefore, no nuclear deformation was observed. MSCs on the micropatterns with different geometries had limited spreading area. The cells exhibited similar disrupt actin structure at perinuclear region although they formed intensive stress fibers at cell edge. The results indicated that the cytoskeletal structure might be an important factor for regulation of cell quiescence which contributes to keeping stem cell phenotype.

The cellular tension which depends on cytoskeletal organization is also important for maintenance of multipotency of stem cells. Previous study reported that round ESCs exhibited higher expression of Oct4 and Nanog than flattened ones due to the weak membrane-cytoskeleton linkages.[34] And limited spreading area was revealed to be beneficial for the maintenance of undifferentiated state of ESCs.[35] Human induced pluripotent stem cells (iPSCs) with weak stress fibers were Oct3/4 positive while those formed pronounced stress fibers became Oct3/4 negative.[36] For MSCs, undifferentiated cells were found to have low contractility compared to osteogenic differentiated cells, indicating the low cytoskeletal tension was required to maintain the multipotency.[37] In this study, the elasticity of MSCs cultured on the micropatterns increased with cellular enlargement which was in good accordance with previous work.[28] Similarly, the parallel stress fibers formed in elongated cells also enhanced the elasticity of MSCs. MSCs with different geometries showed disrupt actin structure at cell center, which leaded to low elasticity. Combined with the staining results, high elasticity of MSCs was always accompanied with low expression of surface molecules suggesting partial loss of multipotency.

Conclusions

In summary, the cell morphogenesis was well controlled by the PSt micropatterns with different size, geometry and aspect ratio. MSCs on the micropatterns showed different expression level of stem cell surface markers, and accompanied with different nuclear activity, cytoskeletal structure and nanomechanics. The micropatterns should directly affect cytoskeletal structures. The resulting cytoskeletal structure

could determine cellular nanomechanics, nuclear activity and stemness of MSCs. Large spreading area and high aspect ratio leaded cells to a stressed state with active nuclear synthesis, and therefore resulted in low expression of stem cell surface markers. When spreading area was limited, changes in cell geometries did not influence cell elasticity and nuclear activity. Ordered cytoskeletal structure resulted in high cell elasticity and nuclear activity and decreased the expression of surface markers indicating partial loss of multipotency. MSCs with disrupt cytoskeletal structure exhibited low nanomechanical properties and retained in a quiescent state which promoted stem cell phenotype.

Acknowledgements

This work was supported by the World Premier International Research Center Initiative on Materials Nanoarchitectonics and JSPS KAKENHI Grant Number 24300177 (Grant-in-Aid for Scientific Research (B)).

References

1 F. P. Barry and J. M. Murphy, *Int. J. Biochem. Cell Biol.*, 2004, **36**, 568-584.
2 M. F. Pittenger, *Science*, 1999, **284**, 143-147.
3 R. McBeath, D. M. Pirone, C. M. Nelson, K. Bhadriraju and C. S. Chen, *Dev. Cell*, 2004, **6**, 483-495.
4 M. J. Dalby, N. Gadegaard, R. Tare, A. Andar, M. O. Riehle, P. Herzyk, C. D. W. Wilkinson and R. O. C. Oreffo, *Nat. Mater.*, 2007, **6**, 997-1003.
5 M. P. Lutolf, P. M. Gilbert and H. M. Blau, *Nature*, 2009, **462**, 433-441.
6 Y. Kunisaki, I. Bruns, C. Scheiermann, J. Ahmed, S. Pinho, D. Zhang, T. Mizoguchi, Q. Wei, D. Lucas, K. Ito, J. C. Mar, A. Bergman and P. S. Frenette, *Nature*, 2013, **502**, 637-643.
7 M. M. Bonab, K. Alimoghaddam, F. Talebian, S. H. Ghaffari, A. Ghavamzadeh and B. Nikbin, *BMC Cell Biol.*, 2006, **7**, 14-21.
8 R. J. McMurray, N. Gadegaard, P. M. Tsimbouri, K. V. Burgess, L. E. McNamara, R. Tare, K. Murawski, E. Kingham, R. O. C. Oreffo and M. J. Dalby, *Nat. Mater.*, 2011, **10**, 637-644.
9 K. C. Rustad, V. W. Wong, M. Sorkin, J. P. Glotzbach, M. R. Major, J. Rajadas, M. T. Longaker and G. C. Gurtner, *Biomaterials*, 2012, **33**, 80-90.
10 S. Gerecht, J. Burdick, L. S. Ferreira, S. Townsend, R. Langer and G. Vunjak-Novakovic, *Proc. Natl. Acad. Sci. U. S. A.*, 2007, **104**, 11298-11303.
11 P. M. Gilbert, K. L. Havenstrite, K. E. Magnusson, A. Sacco, N. A. Leonardi, P. Kraft, N. K. Nguyen, S. Thrun, M. P. Lutolf and H. M. Blau, *Science*, 2010, **329**, 1078-1081.
12 J. H. Wen, L. G. Vincent, A. Fuhrmann, Y. S. Choi, K. C. Hribar, H. Taylor-Weiner, S. Chen and A. J. Engler, *Nat. Mater.*, 2014, **13**, 979-987.
13 P. Y. Wang, H. H. Lee, A. Higuchi, Q. D. Ling, H. R. Lin, H. F. Li, S. S. Kumar, Y. Chang, A. A. Alarfai, M. A. Munusamy, D. C. Chen, S. T. Hsu, H. C. Wang, H. Y. Hsiao and G. J. Wu, *J. Mater. Chem. B*, 2015, **3**, 3858-3869.
14 M. Thery, *J. Cell Sci.*, 2010, **123**, 4201-4213.
15 X. Wang, W. Song, N. Kawazoe and G. Chen, *J. Biomed. Mater. Res. Part A*, 2013, **101A**, 3388-3395.
16 X. Wang, W. Song, N. Kawazoe and G. Chen,. *Soft Matter*, 2013, **9**, 4160-4166.
17 B. Ohler, *Rev. Sci. Instrum.*, 2007, **78**, 063701.
18 K. D. Costa, *Dis. Markers*, 2004, **19**, 139-154.
19 S. Zhang, Z. Jia, J. Ge, L. Gong, Y. Ma, T. Li, J. Guo, P. Chen, Q. Hu, P. Zhang, Y. Liu, Z. Li, K. Ma, L. Li and C. Zhou, *Cell Transplant.*, 2005, **14**, 787-798.
20 M. Dominici, K. Le Blanc, I. Mueller, I. Slaper-Cortenbach, F. Marini, D. Krause, R. Deans, a Keating, D. Prockop and E. Horwitz, *Cytotherapy*, 2006, **8**, 315-317.
21 M. K. Majumdar, M. Keane-Moore, D. Buyaner, W. B. Hardy, M. A. Moorman, K. R. McIntosh and J. D. Moska, *J. Biomed. Sci.*, 2003, **10**, 228–241.
22 D. Docheva, F. Haasters and M. Schieker, *Curr. Rheumatol. Rev.*, 2008, **4**, 155-160.
23 L. Li, H. Clevers, *Science*, 2010, **327**, 542-545.
24 M. Osawa, G. Egawa, S. S. Mak, M. Moriyama, R. Freter, S. Yonetani, F. Beermann and S. I. Nishikawa, *Development*, 2005, **132**, 5589-5599.
25 J. P. Winer, P. Jammey, M. E. McCormick and M. Funaki, *Tissue Eng. Part A*, 2009, **15**, 147-154.
26 A. J. Engler, S. Sen, H. L. Sweeney and D. E. Discher, *Cell*, 2006, **126**, 677-689.
27 K. N. Dahl, A. J. S. Ribeiro and J. Lammerding, *Circ. Res.*, 2008, **102**, 1307-1318.
28 C. Yang, M. W. Tibbitt, L. Basta and K. S. Anseth, *Nat. Mater.*, 2014, **13**, 645-652.
29 P. Roca-Cusachs, J. Alcaraz, R. Sunyer, J. Samitier, R. Farré and D. Navajas, *Biophys. J.*, 2008, **94**, 4984-4995.
30 A. Mammoto, S. Huang, K. Moore, P. Oh and D. E. Ingber. *J. Biol. Chem.*, 2004, **279**, 26323-26300.
31 S. B. Khatau, C. M. Hale, P. J. Stewart-Hutchinson, M. S. Patel, C. L. Stewart, P. C. Searson, D. Hodzic and D. Wirtz, *Proc. Natl. Acad. Sci. U. S. A.*, 2009, **106**, 19017-19022.
32 Q. Li, A. Kumar, E. Makhija and G. V. Shivashankar, *Biomaterials*, 2014, **35**, 961-969.
33 K. Kurpinski, J. Chu, C. Hashi, S. Li. *Proc. Natl. Acad. Sci. U. S. A.*, 2006, **103**, 16095-16100.
34 F. Veraitch, *Cell Health Cytoskelet.*, 2011, **3**, 23-34.
35 D. Bae, S. H. Moon, B. G. Park, S. J. Park, T. Jung, J. S. Kim, K. B. Lee and H. M. Chung, *Biomaterials*, 2014, **35**, 916-928.
36 M. H. Kim and M. Kino-Oka, *Biomaterials*, 2014, **35**, 5670-5678.
37 P. M. Tsimbouri, R. J. McMurray, K. V. Burgess, E. V. Alakpa, P. M. Reynolds, K. Murawski, E. Kingham, R. O. Oreffo, N. Gadegaard and M. J. Dalby, *ACS Nano*, 2012, **6**, 10239-10249.

Photo-reactive PVA micropatterned polystyrene surfaces are prepared by photolithographic micropatterning to control cell spreading, geometry and aspect ratio of single mesenchymal stem cells. The stemness change of MSCs is significantly influenced by cell morphogenesis, and always accompanied with change of nuclear activity and cytoskeleton mediated nanomechanics.